# Supporting Information

# Boron-Doped Spherical Hollow-Porous Silicon Local Lattice Expansion toward a High-Performance Lithium-Ion-Battery Anode

*Yongpeng Ren,*[†] *Xiangyang Zhou,*[†] *Jingjing Tang,*[†] *Jing Ding,*[†] *Song Chen,*[†] *Jiaming Zhang,*[†] *Tingjie Hu,*[†] *Xu-Sheng Yang,*[*, ‡] *Xinming Wang,*[§] *and Juan Yang,*[*, †]

[†] School of Metallurgy and Environment, Central South University, Changsha 410083, China.
[‡] Advanced Manufacturing Technology Research Centre, Department of Industrial and Systems Engineering, The Hong Kong Polytechnic University, Hung Hom, Kowloon, Hong Kong, China
[§] School of Materials Science and Engineering, Xiangtan University, Xiangtan, China

*Corresponding author.

* E-mail: xsyang@polyu.edu.hk, (X. Yang)
* E-mail: j-yang@csu.edu.cn, (J. Yang)

$$\rho_{Si} = \frac{1.305\times10^{16}}{N} + \frac{1.133\times10^{17}}{N\times\left[1+\left(N\times2.58\times10^{-9}\right)^{-0.737}\right]} \qquad \text{S1}$$

$\rho_{Si}$, resistivity of B doped crystal Si, Ω cm

$N$, atomic density of boron atom in Si, $cm^{-3}$

**Table S1** B contents in Si and $SiO_2$ based on ICP-AES measurements and the calculated resistivity values

| | B contents In $SiO_2$(wt%) | B contents In Si (wt%) | Atomic density of B ($cm^{-3}$) | Resistivity (Ω cm) |
|---|---|---|---|---|
| B0 | <0.001 | <0.001 | ~$5\times10^{17}$ | ~0.22 |
| B1 | 0.038 | 0.014 | $0.18\times10^{20}$ | $5.48\times10^{-3}$ |
| B2 | 0.093 | 0.029 | $0.38\times10^{20}$ | $2.86\times10^{-3}$ |
| B-HPSi (B-$HSiO_2$) | 0.16 | 0.057 | $0.74\times10^{20}$ | $1.55\times10^{-3}$ |
| Saturated solution of B (theoretical value) | — | 0.17% | $2.2\times10^{20}$ | $5.49\times10^{-4}$ |

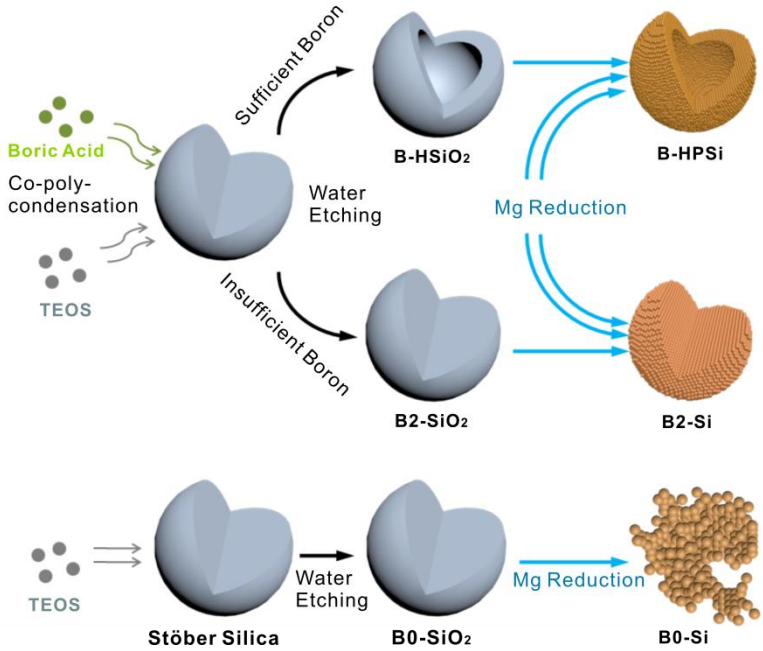


**Figure S1.** Synthetic paths of B-HPSi, B2-Si and B0-Si

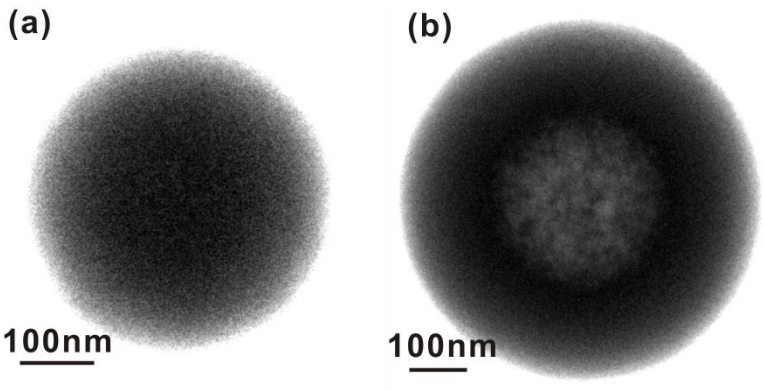


**Figure S2.** Contrast adjusted TEM images of (a) solid silica spheres without boron addition (B0-$SiO_2$) and (b) hollow spheres with proper boron addition (B-$HSiO_2$)

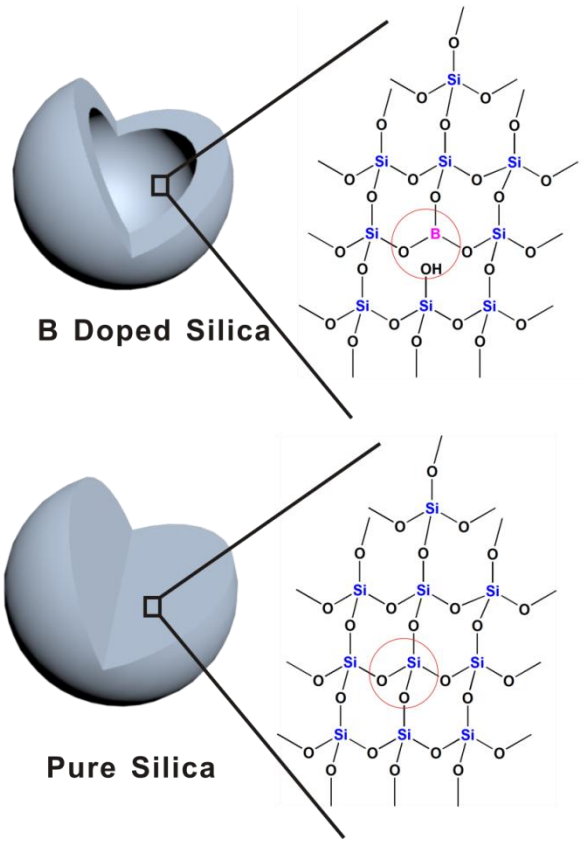


**Figure S3.** Illustration of a boron atom with lower coordination number in Si-O framework

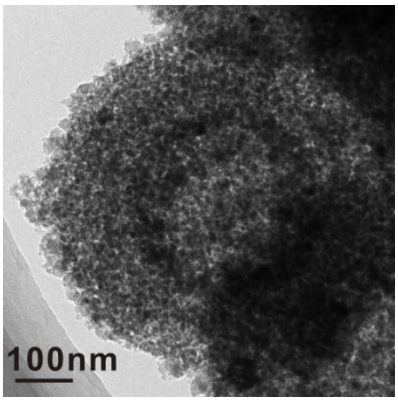


**Figure S4.** Enlarged TEM image of B-HPSi

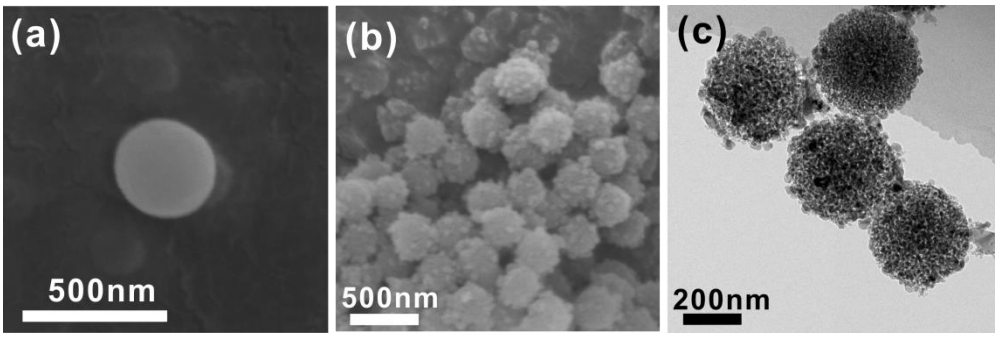


**Figure S5.** SEM images of (a) B2-$SiO_2$, (b) B2-Si and (c) TEM image of B2-Si

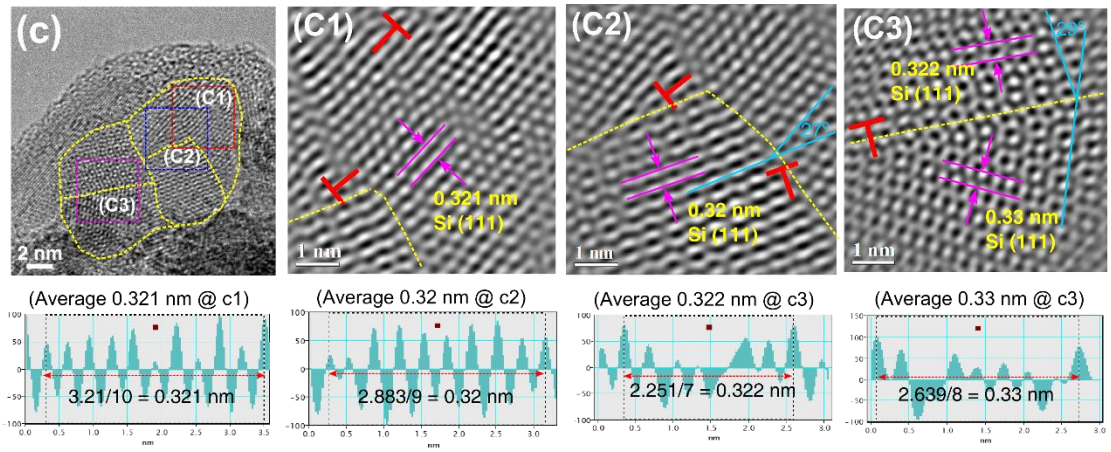


**Figure S6.** HRTEM image of B-HPSi (c) and the Fourier-filtered HRTEM images (C1-C3) enlarged from the rectangular regions marked C1, C2, and C3 in (c); and the corresponding the intensity profiles for measuring the interplanar spacing of Si (111) planes.

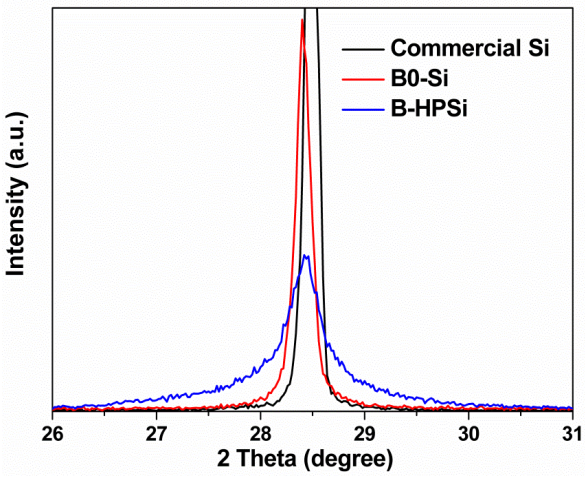


**Figure S7.** Detailed XRD patterns of B-HPSi, B0-Si and commercial Si

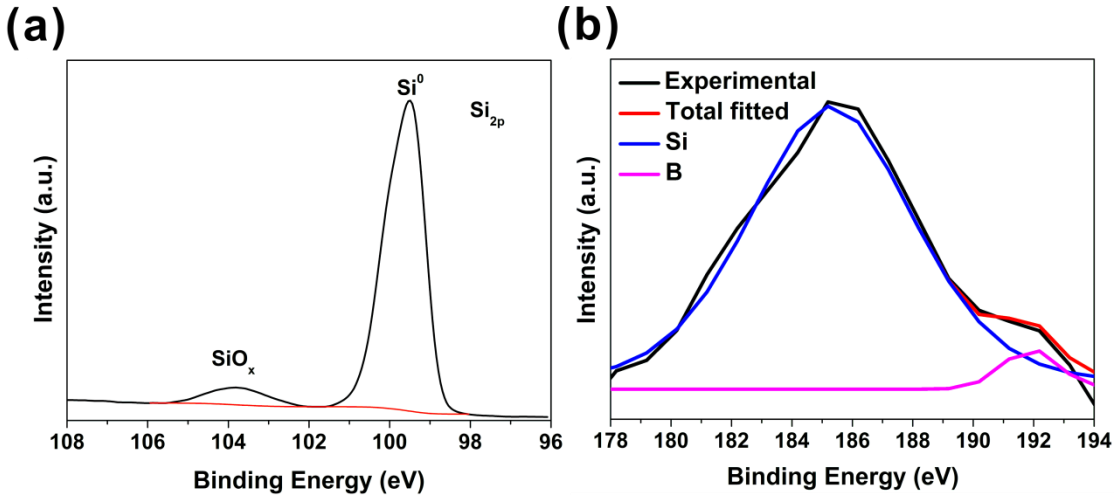


**Figure S8.** (a) Si and (b) B peaks of XPS of B-HPSi

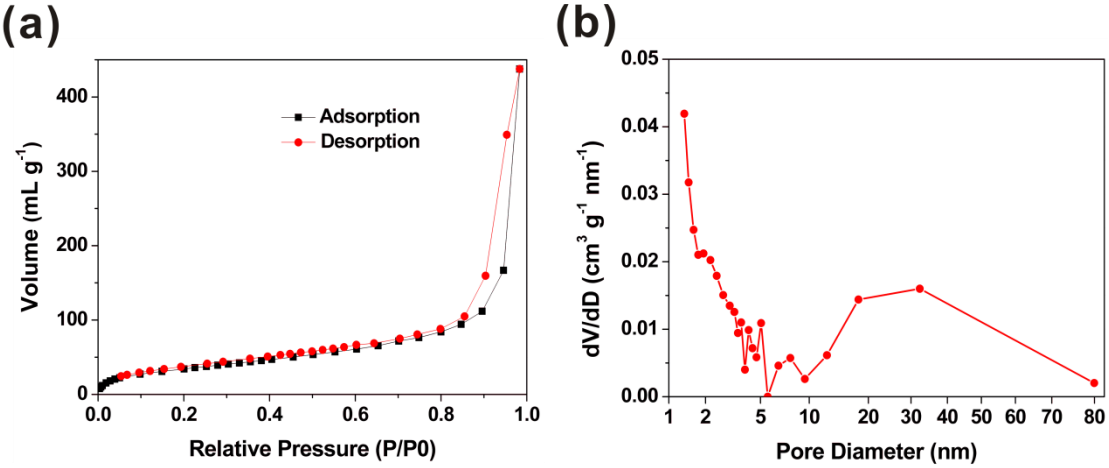


**Figure S9.** N2 adsorption/desorption data (a) and differential pore size distribution (b) of B-HPSi

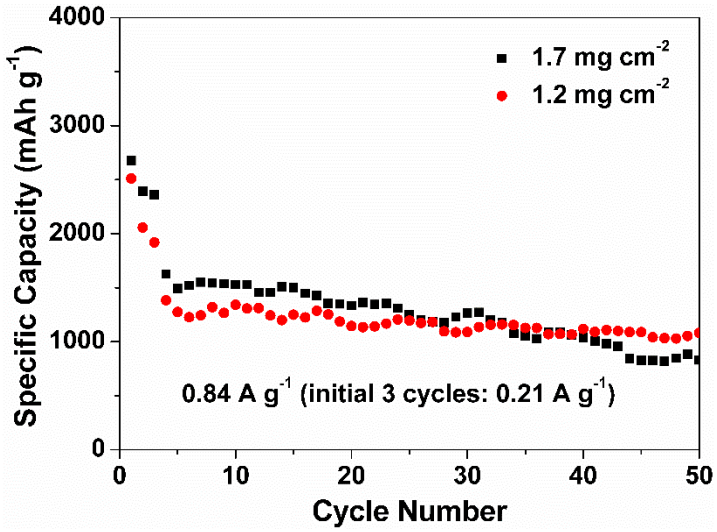


**Figure S10.** Cyclic performances of B-HPSi under areal mass loading of 1.2 mg $cm^{-2}$ and 1.7 mg $cm^{-2}$

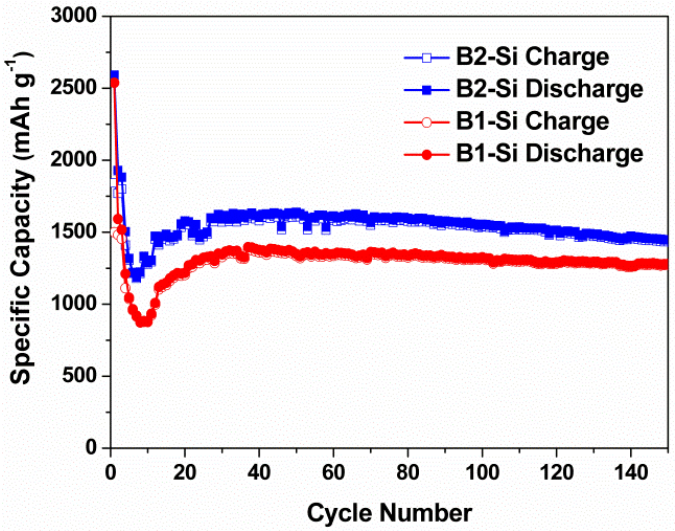


**Figure S11.** Cycle performances at 0.84A $g^{-1}$ of B1-Si and B2-Si (activated at 0.21 A $g^{-1}$ for the initial 3 cycles)

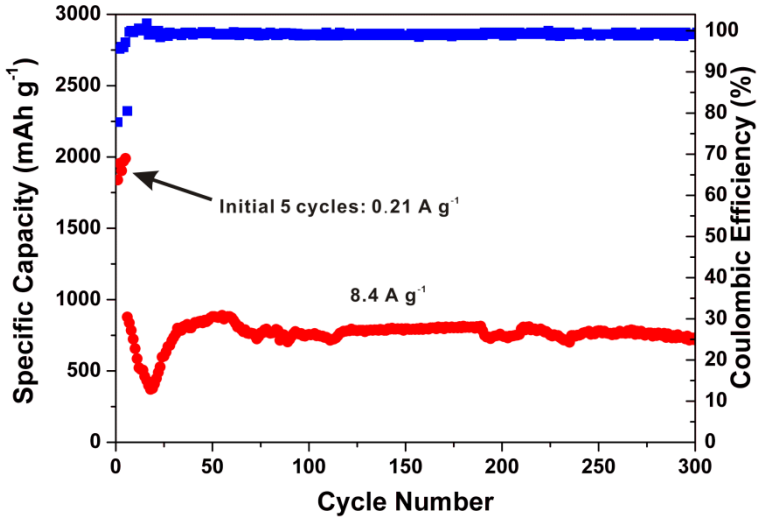


**Figure S12.** Cyclic performances of B-HPSi at 8.4 A $g^{-1}$ (activated at 0.21 A $g^{-1}$ for the initial 5 cycles)

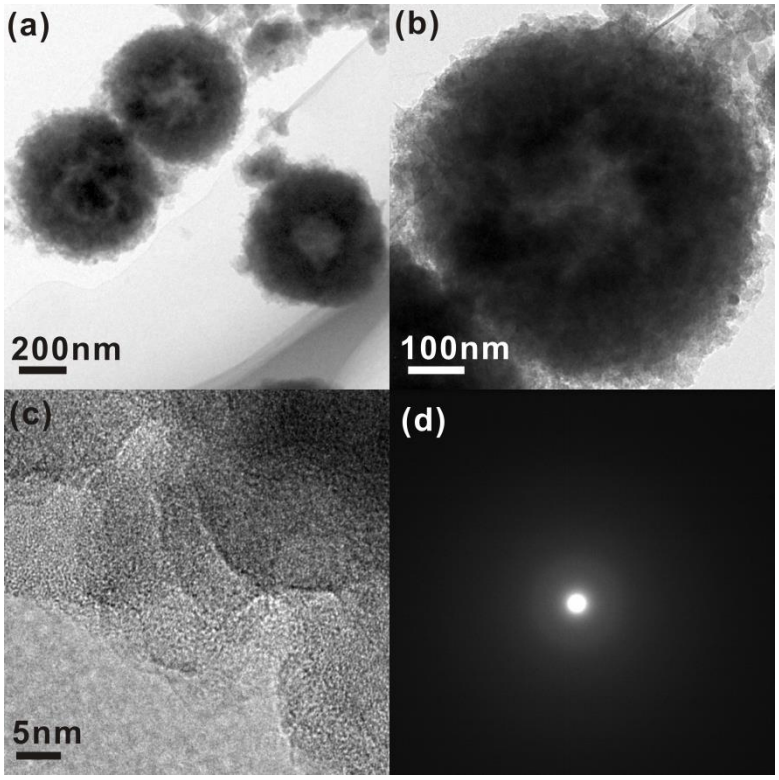


**Figure S13.** TEM (a) and (b), HRTEM (c) and SAED (d) of B-HPSi anode obtained after cycling

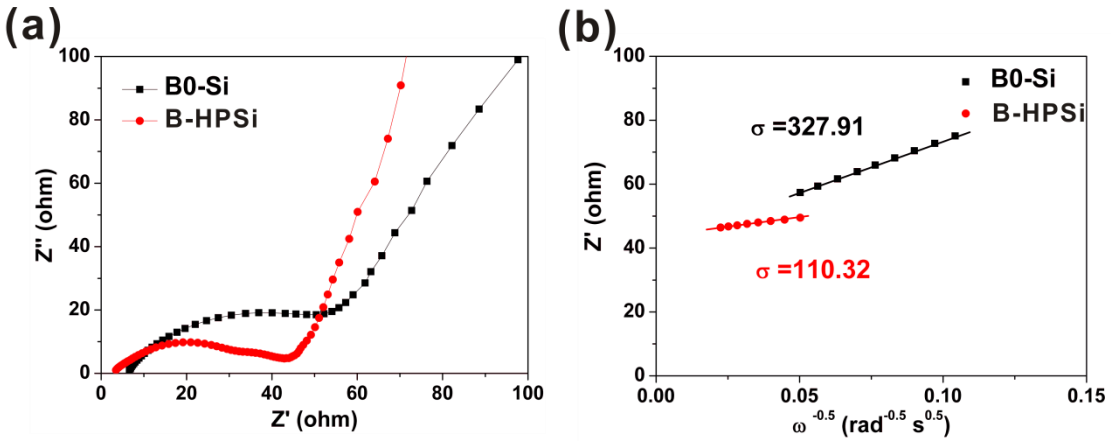


**Figure S14.** Nyquist plots (a) and Warberg coefficients (b) of B-HPSi and B0-Si

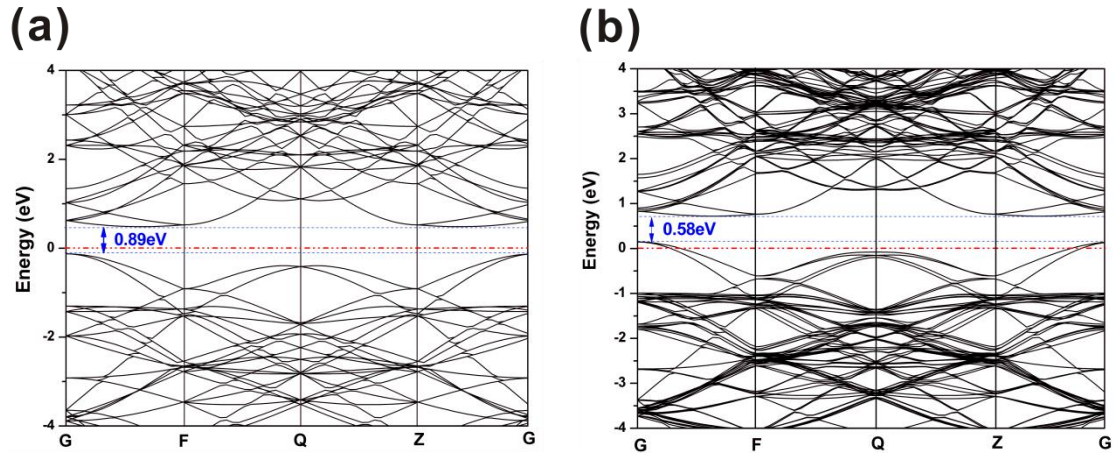


**Figure S15.** Simulated band structure of pure Si (a) and B-doped Si (b)

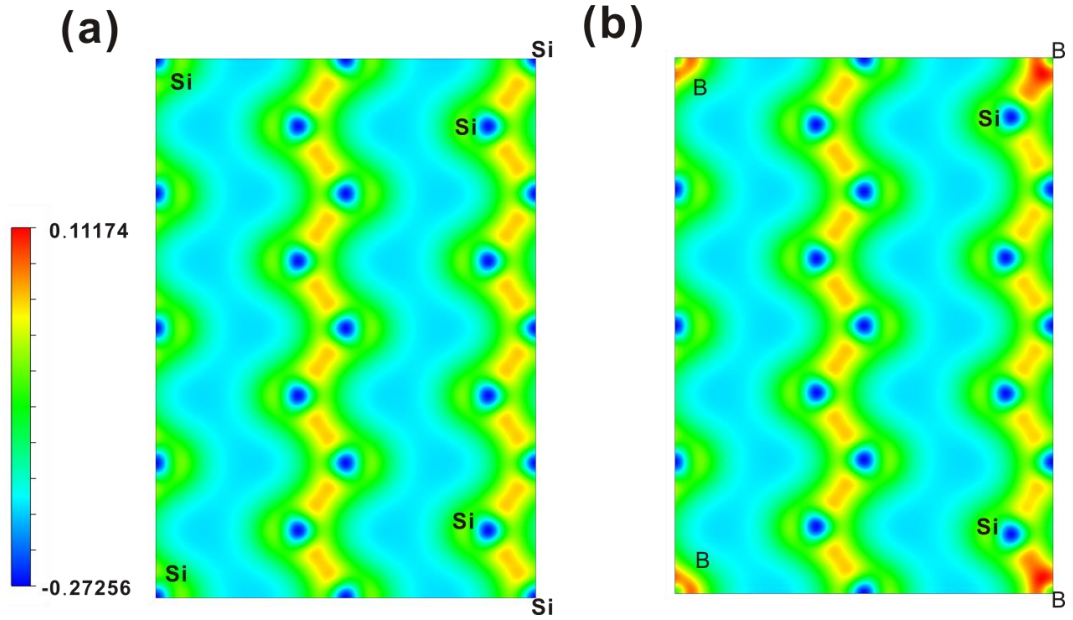


**Figure S16.** Simulated charge density plots of pure Si (110) (a) and B doped Si (110) (b)